Impaired TGFβ Signaling in Plaque-Associated Microglia

Oliver Krzyzan , Angela Kuhla , Björn Spittau , Natascha Vidovic *

Posted Date: 9 December 2025

doi: 10.20944/preprints202512.0809.v1

Keywords: Alzheimer's disease; microglia; TGF-β; SMAD proteins; APP/PS1; neuroinflammation; 3D morphology; confocal microscopy

Article

Impaired TGFβ Signaling in Plaque-Associated Microglia

Oliver Krzyzan [1], Angela Kuhla [2,3], Björn Spittau [4] and Natascha Vidovic [4,*]

[1] Institute of Anatomy and Physiology, University Medicine, Rostock University, Rostock, Germany
[2] Rudolf-Zenker Institute of Experimental Surgery, Rostock Medical Center Rostock University, Rostock, Germany
[3] Centre for Transdisciplinary Neurosciences Rostock (CTNR), Rostock University Medical Centre, Gehlsheimerstraße 20, 18147 Rostock, Germany
[4] Anatomy and Cell Biology, Medical School OWL, Bielefeld University, 33615 Bielefeld, Germany
* Correspondence: natascha.vidovic@uni-bielefeld.de

Abstract

Aging and Alzheimer's disease are associated with profound changes in glial cell morphology and signaling. This study investigates the three-dimensional morphology of microglia and the intracellular localization of phosphorylated SMAD proteins as downstream effectors of TGF-β signaling in the APP/PS1 transgenic mouse model of Alzheimer's disease. Using confocal microscopy and the Simple Neurite Tracer software, we reconstructed and quantitatively analyzed glial cell morphology in aged wild-type and APP/PS1 mice. Immunofluorescence staining revealed altered pSMAD2 and pSMAD1/5/8 distribution in microglia, suggesting impaired canonical TGF-β and BMP signaling. Our findings indicate a disturbed glial morphology and dysfunctional TGF-β signaling cascade in the APP/PS1 model, underlining their potential role in Alzheimer's disease pathogenesis.

Keywords: Alzheimer's disease; microglia; TGF-β; SMAD proteins; APP/PS1; neuroinflammation; 3D morphology; confocal microscopy

1. Introduction

The progressive neuroinflammation observed in aging and neurodegenerative diseases such as Alzheimer's disease (AD) is increasingly linked to both functional and morphological changes in glial cells. Microglia and astrocytes are central to maintaining central nervous system (CNS) homeostasis and respond dynamically to pathological stimuli, including β-amyloid (Aβ) accumulation [1]. One of the key regulatory pathways influencing glial function is mediated by transforming growth factor-beta (TGF-β), particularly via SMAD signaling [2,3]. However, it remains unclear how this pathway—especially the phosphorylation and distribution of SMAD proteins—changes in glia during aging and AD. The present study addresses this gap by examining glial morphology and intracellular TGF-β signaling in aged and APP/PS1 mice, with a focus on phosphorylated SMAD localization.

AD poses a growing global health challenge. Since 1990, its incidence and prevalence have risen markedly, and projections indicate a continued increase through 2040 [4]. The disease typically begins decades before clinical symptoms: biomarkers such as Aβ and neurofilament light chain may rise as early as 20 years prior to diagnosis [5,6]. Recent work has expanded our understanding of AD pathogenesis to include not only protein aggregation but also synaptic dysfunction and altered synaptic plasticity [7].

Aβ peptides—especially the aggregation-prone $A\beta_{42}$—arise from sequential cleavage of amyloid precursor protein (APP) by β-secretase (BACE1) and γ-secretase. In AD, aberrant APP processing favors Aβ overproduction, leading to self-assembly into soluble oligomers, protofibrils, and eventually extracellular plaques. These species impair synaptic plasticity, disrupt neuronal calcium homeostasis, and trigger inflammatory cascades [8] .

 doi:10.20944/preprints202512.0809.v1

In addition to direct amyloid toxicity, increasing evidence implicates neuroinflammation as a driver of both the onset and progression of AD [9]. Neuroinflammation involves activation of the brain's innate immune system in response to stimuli such as misfolded or aggregated proteins [10]. A key consequence is disruption of the blood–brain barrier, enabling infiltration of peripheral immune cells and, in some cases, pathogens into the CNS. This phenomenon occurs not only in AD but also during normal aging, where low-grade inflammation may create a permissive environment for pathology. In amyloid contexts, inflammation both responds to and exacerbates disease processes [11].

Microglia are the brain's resident immune cells, responsible for continuous surveillance of the CNS microenvironment. In their homeostatic state, they support neuronal function through synaptic pruning, debris clearance, and release of trophic factors. Upon encountering pathological stimuli—such as aggregated Aβ—microglia undergo profound morphological and transcriptional changes, shifting from a ramified, surveillant state to an activated phenotype. This activation is accompanied by altered motility, increased phagocytic capacity, and secretion of pro- and anti-inflammatory mediators.

While acute microglial activation can be protective—facilitating removal of harmful aggregates—chronic activation is associated with sustained inflammation, oxidative stress, and synaptic dysfunction. In AD, microglial activation clusters spatially around Aβ plaques, where cells adopt specialized phenotypes to engage with the aggregated material. Emerging evidence suggests that microglial responses are highly heterogeneous, encompassing both beneficial and detrimental effects on disease progression depending on activation state, local environment, and signaling cues such as TGF-β [3].

TGF-β, in particular TGF-β1, is a key regulator of microglial development, homeostasis and reactivity in the central nervous system. TGF-β1 signaling is required for proper microglial maturation and for maintaining a homeostatic, non-inflammatory phenotype in the adult brain, and disruption of TGF-β signaling in microglia leads to abnormalities in microglial number, morphology and gene expression, as well as neurodegeneration [2,12]. In AD, however, TGF-β signaling becomes dysregulated: ligand and receptor levels are altered, and downstream SMAD signaling is modified in ways that can both limit and promote neuroinflammatory responses and amyloid pathology [13]. How canonical TGF-β/SMAD2/3 and BMP/SMAD1/5/8 branches are differentially engaged or impaired in microglia during amyloid-β pathology remains poorly understood and is a key focus of the present study.

In the canonical TGF-β pathway, signal propagation critically depends on the nucleo-cytoplasmic shuttling of SMAD proteins. In the resting state, R-SMADs continuously cycle between cytoplasm and nucleus, with the equilibrium biased toward the cytoplasm, whereas SMAD4 is more evenly distributed. Ligand-induced phosphorylation of R-SMADs promotes formation of SMAD2/3–SMAD4 or SMAD1/5/8–SMAD4 complexes, which accumulate in the nucleus and, together with additional transcription factors, drive target gene transcription. Nuclear export requires complex dissociation and dephosphorylation of R-SMADs, a comparatively slow step that favors transient nuclear accumulation of pSMADs under physiological conditions. Consequently, alterations in the balance between cytoplasmic and nuclear pSMAD provide a sensitive readout of disturbed TGF-β/SMAD signaling in aging and neurodegeneration [14,15].

Single-cell transcriptomic studies have identified a unique microglial phenotype—disease-associated microglia (DAM)—in neurodegenerative diseases [16]. DAM show downregulation of homeostatic genes (e.g., *P2ry12*, *Tmem119*) and upregulation of genes linked to phagocytosis, lipid metabolism, and inflammatory signaling (e.g., *Apoe*, *Trem2*, *Tyrobp*) [17]. DAM activation proceeds in two stages: an initial *Trem2*-independent phase, followed by a *Trem2*-dependent phase that enhances the microglial response to aggregated proteins such as Aβ and hyperphosphorylated tau. While DAM may aid clearance of pathological aggregates, they also contribute to chronic inflammation and synaptic dysfunction [18].

The APP/PS1 transgenic mouse model expresses human mutant APP (the Swedish mutation K670N/M671L) and mutant presenilin-1 (PS1; e.g., L166P or M146L). These mutations increase β-

 doi:10.20944/preprints202512.0809.v1

secretase cleavage, enhance $A\beta_{42}$ production, and accelerate amyloid deposition [19]. APP/PS1 mice develop cortical and hippocampal plaques from 6–7 months onward, accompanied by activated microglia, astrocytosis, and an inflammatory milieu. They also display synaptic and cognitive deficits—including impaired long-term potentiation (LTP) and spatial learning—before major neuronal loss [20]. Notably, DAM-like phenotypes emerge alongside amyloid deposition, making APP/PS1 mice well-suited to studying both amyloid-driven and immunological components of AD [21].

By combining morphological analysis of glia with intracellular mapping of phosphorylated SMAD proteins in aged and APP/PS1 brains, this study aims to clarify whether age- and disease-related inflammatory environments alter TGF-β signaling in ways that could contribute to AD progression.

2. Materials and Methods

2.1. Materials

2.1.1. Anaesthetics and Chemicals

Mice were deeply anaesthetised by an intraperitoneal injection of ketamine (75 mg/kg) and Rompun (5.8 mg/kg). Paraformaldehyde (PFA), Phosphate-buffered saline (PBS) and citrate solution and Triton X-100 were from Sigma, St. Louis, Missouri, US. Copper (II) sulfate was from Merck, Søborg, Denmark. Mounting medium was from Thermo Fisher Scientific, Waltham, Massachusetts, US. DAPI was from Roth, Karlsruhe, Germany. Chemicals otherwise used were of the purest grade available from regular commercial sources.

2.1.2. Antibodies

Table 1. Primary antibodies.

Antibody	Clonality	Dilution	Species	Producer	Catalog No.
β-Amyloid	mono	1:1000	Mouse	BioLegend	803001
Iba-1	poly	1:500	Guinea pig	Synaptic Systems	234004
Iba-1	poly	1:500	Rabbit	Wako	019-19741
TGF-β1	poly	1:50	Rabbit	Santa Cruz	sc-146
pSMAD2	poly	1:200	Rabbit	Invitrogen	44-244C
pSMAD1/5/8	mono	1:800	Rabbit	Cell Signaling	13820

Table 2. Secondary antibodies.

Target	Species	Dilution	Conjugate	Producer	Catalog No.
Mouse	Goat	1:500	Alexa Fluor™ 488	Abcam	ab150113
Guinea pig	Goat	1:500	Alexa Fluor™ 488	Abcam	ab150185
Rabbit	Goat	1:500	Alexa Fluor™ 594	Abcam	ab150080
Rabbit	Goat	2 gtt/ml	Alexa Fluor™ 594	Invitrogen	R37117
Mouse	Goat	1:200	Alexa Fluor™ 594	Abcam	ab150116

2.2. Animals

The present study was carried out in accordance with the European Communities Council Directive of September 22nd 2010 (2010/63/EEC) for care of laboratory animals. The breeding was approved by the of the local Animal Research Committee (Landesamt für Landwirtschaft, Lebensmittelsicherheit und Fischerei (LALLF)) of the state Mecklenburg-Western Pomerania (LALLF M-V/TSD/7221.3-2-034/17).

Three young wildtype (female, 6 months), four aged wildtype (female, 24 months old) and five aged APP/PS1 mice (female, 24 months old) (stock# 034829, Jackson Laboratory, Bar Harbor, ME, USA) were used in in accordance to §4 (german animal welfare act, version from 2017) and were

 doi:10.20944/preprints202512.0809.v1

sacrificed by cervical dislocation in deep anesthesia (ketamine/rompun). The dead mice were decapitated in order to remove brain tissue. APP/PS1 mice express both chimeric amyloid precursor protein (human APP695swe) with Swedish double mutations (K595N/M596L) and human presenilin protein 1 carrying the exon-9-deleted variant (PS1-dE9) [22]. Additional information at: https://www.jax.org/strain/004462. Mice had free access to food and water and were housed in a 12 h light/dark cycle. The health status of the mice was checked daily.

2.3. Tissue Preparation, Immunohistochemistry and Image Acquisition

After decapitation, brains were fixed in 4% PFA for 24 h, then washed in PBS for 10 min and at last cryoprotected in 30% sucrose for 72 h. Finally, the brains were stored at -80 °C until cryostat sectioning. Coronal brain slices (50 µm) were cut using a cryostat (CM 3050 S, Leica Microsystems, Wetzlar, Germany) and stored in PBS at 4°C. Immunofluorescence involved different double-stainings for Aβ, Iba-1 (rabbit, from Wako), TGF-β1, pSMAD2 and pSMAD1/5/8 with DAPI as a counterstain. Brain slices from the frontal lobe were processed over three days. Primary and secondary antibodies were applied sequentially, with all steps conducted under reduced light exposure. To reduce lipofuscin autofluorescence, sections were finally treated with a solution of 35 mM $CuSO_4$ in 50 mM ammonium acetate buffer (pH 5) for 1 h after antibody staining and washed afterwards with PBS to remove any residues of $CuSO_4$. Sections from young and old animals were treated equally, as $CuSO_4$ solution can also reduce intensities of immunofluorescent labeling [23]. Stained slices were mounted on glass slides and stored at 4 °C. Fluorescence microscopy was performed using a Nikon C1 confocal system with a Nikon PCM-2000 confocal microscope scanning system coupled to an ECLIPSE E400 microscope. Images (Z-Stacks) were captured in 1024p and processed in Nikon EZ-C1 Software. Exposure times were optimized per image to prevent overexposure, and images were taken at 60×magnification across multiple regions of interest (ROI) in the frontal cortex and white matter.

2.4. Data Analysis

2.4.1. Quantification and Cell Morphology

Histological quantification was conducted using Fiji. Cells and Aβ-Plaques were counted in Maximal Intensity Projections (MIP) of the Z-Stacks and their number was then related to the volume of the data set. Microglia and astrocyte morphology was examined using a Sholl-Analysis. For this purpose, each individual cell was first reconstructed in a semi-automated procedure using a Fiji plugin called Simple Neurit Trace (SNT) [24]. For a reconstruction as complete as possible, a preselection of the cells was made:

(1). A soma with DAPI signal should be recognizable.

(2). Processes should not be cut off in the x- and y-axis by image borders.

(3). The cell should be as central as possible in relation to the z-axis in order to reconstruct extensions in this plane as well as possible.

(4). It should be possible to differentiate between neighboring cells in order to be able to assign extensions as clearly as possible to a cell.

For better demarcation of the processes. Before using SNT a Background Subtraction was performed and Brightness/Contrast was elevated. After reconstruction, finally, a Traces File gives information about every single reconstructed process, so the sum could be calculated. From the reconstructed cell, a skeletal rendering could be created from which information about the number of branches and endpoints could be obtained. A Sholl analysis was also created. The number of primary processes and the maximum number of processes crossing a certain radius could be taken from the Sholl results file and the Schoenen ramification index (SRI) could be determined. The surface area was measured manually as a convex hull. For the measurement of the soma, Z-stacks of the native images were used as a maximum projection. The area covered by processes was measured using the SNT-reconstructions.

 doi:10.20944/preprints202512.0809.v1

2.4.2. Quantification of Fluorescence Intensities

The fluorescence intensities were also quantified using Fiji. First, the integrated density of the ROI fluorescence and the area of the ROI were measured. The integrated density is the product of the measured area and the average gray value. The average gray value is the sum of the gray values of all the pixels in the selection divided by the number of pixels. In addition to the ROI, five further intensities were measured above the background of the image and an average value was calculated. A corrected total cell fluorescence (CTCF) could then be calculated: CTCF = Integrated density - (area of ROI * average background intensity) [25]. For measurements of nuclear intensities, the DAPI signal was used as ROI. For measurements of the cytoplasm of microglia, the ROI was defined by the Iba-1 signal and the DAPI signal. Microglia processes were not part of the ROI.

2.4.3. Statistical Analyses

The statistical analysis was carried out using Excel and GraphPad PRISM 10.4.0. Outliers of the individual values of each cell were not taken into account in the further calculation, as they could be caused by possible measurement errors. Outliers were defined as values that were more than two standard deviations away from the mean value. Mean values for each animal were calculated from the remaining values collected from individual cells. Three groups were always compared: 6 months WT, 24 months WT and 24 months AD. The samples were first examined for normal distribution using the Shapiro-Wilk test. For normally distributed data with comparable variances, group differences were assessed by one-way ANOVA followed by Tukey's multiple comparisons test. For non-normally distributed data, the Kruskal–Wallis test followed by Dunn's multiple comparisons test was used. P values < 0.05 were considered statistically significant (*$p < 0.05$, *$p < 0.01$, ***$p < 0.001$; ns, not significant). Data are presented as mean ± SEM, with each dot representing the mean value of one animal.

2.4.4. Bulk RNA-Seq Data Acquisition and Processing

Publicly available bulk RNA-sequencing (RNA-seq) data of microglia from amyloid-β mouse models were re-analyzed to complement our histological findings. Raw count matrices and metadata were obtained from [26], accession GSE205048. Gene-level expression values (pseudocounts) for all expressed genes were obtained from Table S3 of the supplementary material, which contains bulk transcriptome profiles of three microglial populations: control microglia (CM), plaque-distant microglia (PCM) and plaque-associated microglia (PAM), sampled at 8 and 12 months of age.

Microglia were identified based on canonical marker expression (P2ry12, Tmem119) and subclustered into homeostatic and disease-associated states.

For descriptive comparison across groups, we calculated gene-wise means for CM, PCM and PAM at each time point. Where indicated, values were $\log_2$-transformed after adding a small offset to avoid taking the logarithm of zero. We focused on curated gene sets comprising components of the TGF-β–SMAD pathway, including ligands (*Tgfb1–3*), receptors (*Tgfbr1, Tgfbr2*), R-/co-/I-SMADs (*Smad1, Smad2, Smad3, Smad4, Smad5, Smad7, Smad8*), and representative downstream target genes. No additional normalization beyond the pseudocount transformation provided by the original authors was applied, and all analyses were restricted to the microglial samples defined in the original study.

3. Results

3.1. Amyloid Burden

To verify that the 24-month-old APP/PS1 mice display the amyloid pathology, the number of amyloid plaques and their size was quantified by immunostaining (Figure 1). Immunostaining results confirmed extensive cortical Aβ plaque formation in 24-months-old APP/PS1 mice. Quantification of plaque density (per mm^3) and mean plaque diameter confirms robust cortical

 doi:10.20944/preprints202512.0809.v1

amyloid pathology in APP/PS1 mice, thereby validating the model for subsequent downstream analyses.

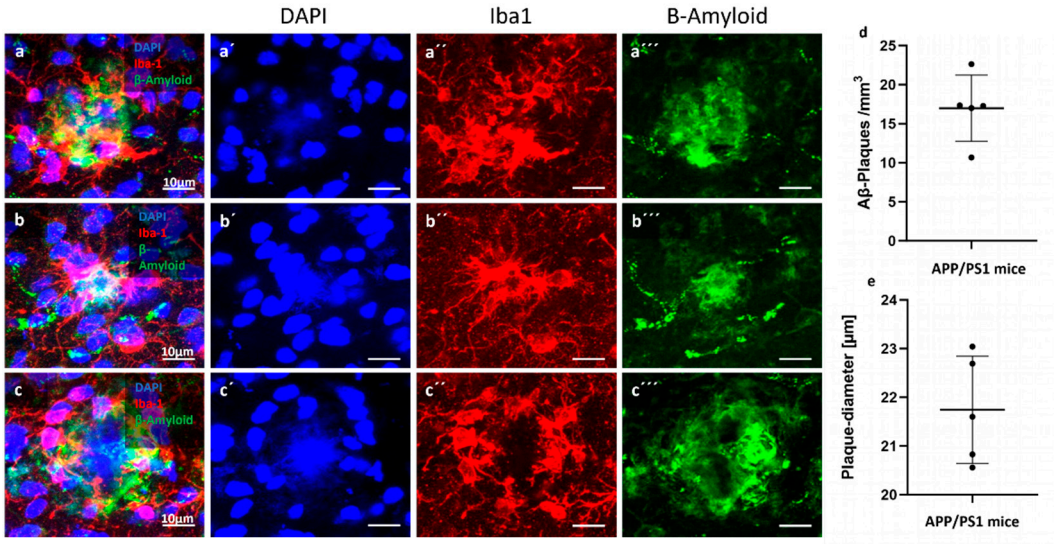

Figure 1. Amyloid-β plaque distribution and quantification in the cortex of APP/PS1 mice. (a–c) Representative immunofluorescence images showing Aβ plaques (green) in the cortical region of 24-month-old APP/PS1 mice. Nuclei are counterstained with DAPI (blue). Microglia are stained with Iba-1 (red). (d) Density of amyloid-β (Aβ) plaques per mm³ in the cortical region of 24-month-old APP/PS1 mice. Each dot represents one animal; horizontal bars indicate the mean ± SEM. (e) Mean plaque diameter (in µm) across cortical Aβ plaques measured per animal. Data show relatively consistent plaque size with moderate variability across individuals. Measurements were obtained from immunofluorescence-labeled sections using confocal microscopy.

3.2. Glial Cell Density in the Brain of Aged WT and APP Mice

Next, we investigated the glial response to amyloid deposition. Immunostaining for the microglial marker Iba-1 demonstrated a marked increase in microglial density in 24-month-old APP/PS1 mice compared to both 6-month and 24-month-old WT groups, whereas no significant difference was observed between young and aged WT mice (Figure 2*a–b*). This indicates that microgliosis in the APP/PS1 cortex is primarily driven by amyloid pathology rather than aging alone.

To further assess microglial alterations, we performed 3D reconstructions and Sholl analyses of Iba-1⁺ cells. Morphological evaluation revealed highly ramified structures in 6-month WT animals, moderate simplification in aged WT mice, and a hypertrophic, amoeboid phenotype with retracted processes in APP/PS1 mice (Figure 3a). Sholl profiles confirmed an age-dependent reduction in arbor complexity, with APP/PS1 microglia displaying the smallest maximum radius (42 µm vs. 62 µm in WT, Figure 3b). Interestingly, microglia from APP/PS1 mice exhibited an increased number of primary processes at the soma, resulting in an early peak of intersections at 10–14 µm.

Microglia from 6-month-old WT animals exhibit the highest number of intersections, indicating greater arbor complexity. Both aged WT and APP/PS1 microglia show markedly reduced branching, particularly in distal regions, reflecting age- and disease-associated morphological simplification. Furthermore, the Sholl analysis indicates that microglia in the AD group possess a higher number of primary processes, as evidenced by an increased number of intersections at a radius of 1 µm. These primary processes subsequently branch out, resulting in a peak number of intersections at a radius of 10–14 µm in all groups. Regarding the number of primary processes, the 6-month WT group shows the greatest increase in intersections, whereas the AD group exhibits only a modest rise (Figure 3).

 doi:10.20944/preprints202512.0809.v1

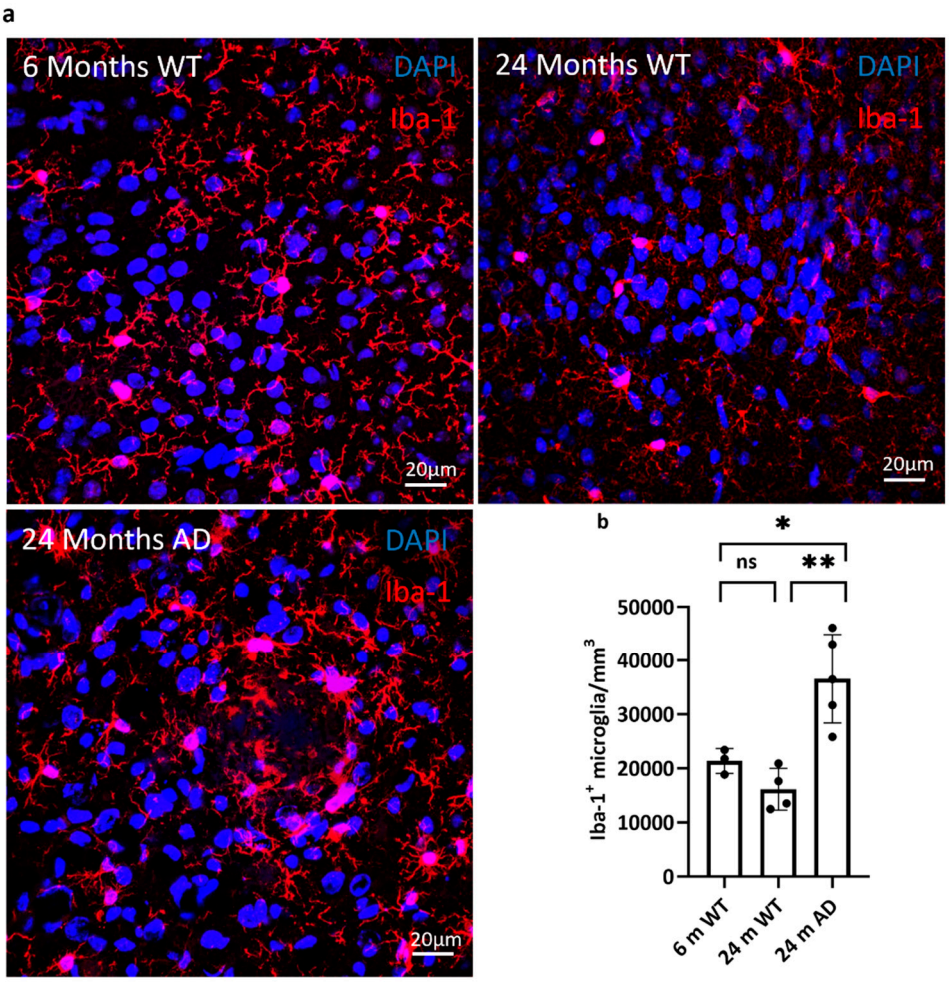

Figure 2. Increased microglial density in the cortex of aged APP/PS1 mice. (a) Representative confocal images showing Iba-1 immunostaining (red) for microglia in the cortex of 6-month-old wild-type (WT), 24-month-old WT, and 24-month-old APP/PS1 (AD) mice. Nuclei are counterstained with DAPI (blue). Scale bar: 20 µm. An increase in Iba-1⁺ microglial density is evident in the 24-month AD group compared to age-matched controls. (b) Quantification of Iba-1⁺ microglia per mm³ reveals a significant increase in the 24-month APP/PS1 group compared to both 6-month and 24-month WT mice. Statistical significance was assessed by one-way ANOVA with Tukey's post hoc test: $p < 0.05$, $p < 0.01$; ns: not significant; n = 3–4 per group. Data are presented as mean ± SEM.

Quantitative analysis of morphological parameters further supported these observations (Figure 4). The number of branch points, endpoints, and the ramification index were highest in 6-month WT microglia and significantly reduced in both aged WT and APP/PS1 mice, with no additional decrease in the AD group compared to age-matched controls (Figure 4*c*).

The number of branch points per cell was significantly higher in 6-month-old WT mice compared to both 24-month-old WT and APP/PS1 mice (Figure 4a; $p < 0.05$ and $p < 0.01$, respectively), indicating a decline in process arborization with aging and disease. Notably, no significant difference was observed between aged WT and APP/PS1 groups (*ns*).

Similarly, the number of endpoints (Figure 4*b*), representing the terminal extensions of microglial processes, was significantly reduced in both 24-month-old groups compared to young WT ($p < 0.05$), with no further reduction in APP/PS1 mice.

The ramification index, a measure of process complexity relative to cell size, was also highest in young WT animals and significantly lower in aged APP/PS1 mice (Figure 4c; $p < 0.05$), further supporting a simplification of microglial morphology during aging.

 doi:10.20944/preprints202512.0809.v1

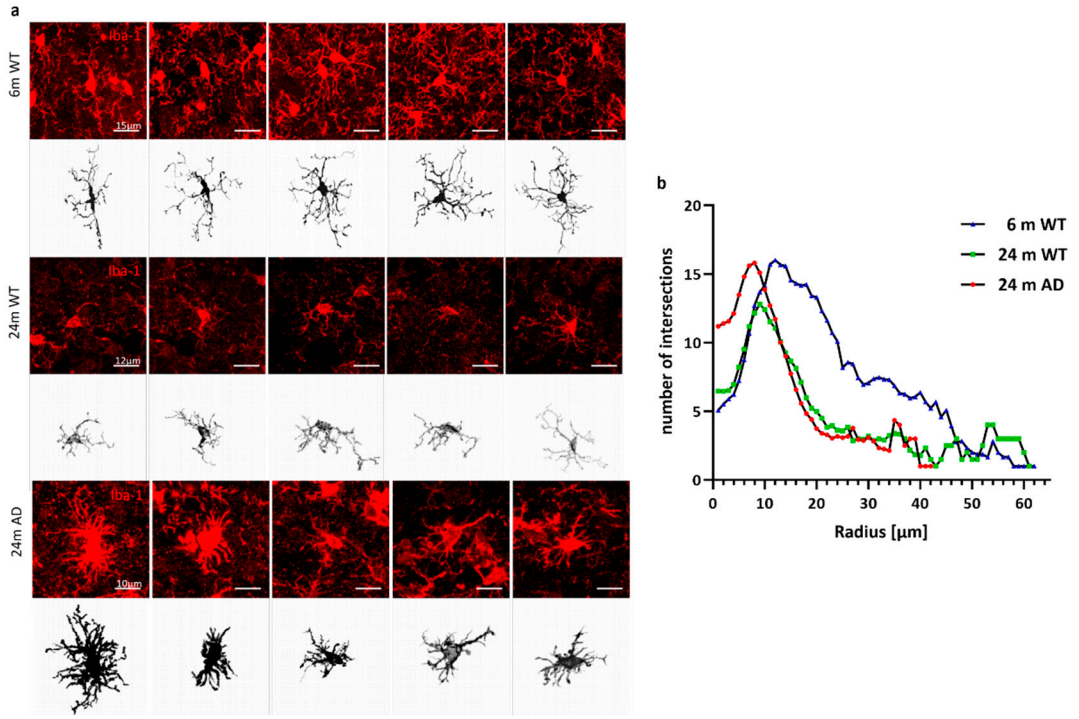

Figure 3. Representative microglial morphologies across experimental groups. (a) Iba-1 immunostaining (red) and corresponding 3D reconstructions (black) of individual cortical microglia from 6-month-old wild-type (top rows), 24-month-old wild-type (middle rows), and 24-month-old APP/PS1 (bottom rows) mice. Scale bars: 15 µm (top), 12 µm (middle), and 10 µm (bottom). (b) Sholl analysis reveals reduced microglial arbor complexity in aged and APP/PS1 mice. Line graph showing the number of process intersections with concentric spheres (Sholl radii) at increasing distances from the soma center of microglia in 6-month-old wild-type (WT, blue), 24-month-old WT (green), and 24-month-old APP/PS1 (AD, red) mice. Data represent mean values per radius step from n ≥ 3 animals per group.

Collectively, these findings highlight an age-dependent reduction in microglial complexity, with APP/PS1 mice showing similar levels of morphological simplification as their age-matched wild-type counterparts.

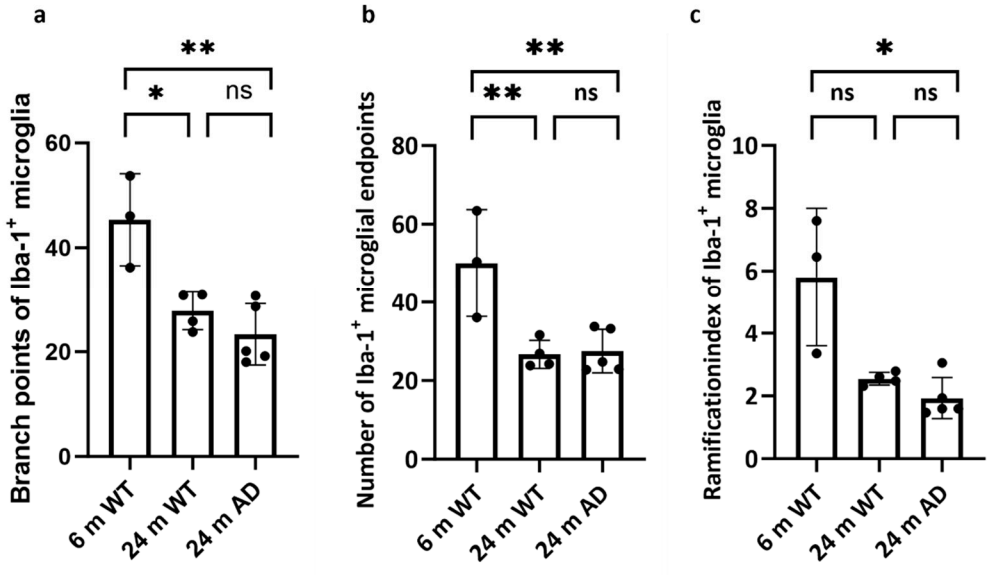

Figure 4. Quantitative analysis of microglial morphology reveals age- and disease-associated simplification. Bar graphs showing (a) the number of branch points, (b) number of endpoints, and (c) the ramification index of

 doi:10.20944/preprints202512.0809.v1

individual Iba-1⁺ microglia in 6-month-old wild-type (WT), 24-month-old WT, and 24-month-old APP/PS1 (AD) mice. Statistical significance was assessed by one-way ANOVA with Tukey's post hoc test. The ramification index of Iba-1⁺ microglia was analyzed using a Kruskal–Wallis test followed by Dunn's multiple comparisons test, because data did not meet the assumptions of normality required for parametric testing: $p < 0.05$, $p < 0.01$, ns = not significant. Data are presented as mean ± SEM, n = 4–5 mice per group.

3.3. TGF-b Signaling

We next examined TGF-β pathway activity in microglia. Immunostaining confirmed TGF-β1 expression in glial populations (Figure 5). Quantitative analysis of TGF-β1 immunoreactivity in Iba-1⁺ microglia revealed a disease-related increase in signal intensity. Microglia from 24-month WT mice showed a modest elevation of TGF-β1 corrected total cell fluorescence (CTCF) compared with 6-month WT animals, but this difference did not reach statistical significance (ns). In contrast, microglia from 24-month APP/PS1 mice displayed a robust increase in TGF-β1 CTCF, with values clearly exceeding both 6-month WT and age-matched 24-month WT levels. Despite some inter-animal variability, all APP/PS1 mice showed consistently higher TGF-β1 signal in microglia, indicating a pronounced upregulation of microglial TGF-β1 expression in the aged AD-like brain. Group-wise comparisons (one-way ANOVA with post-hoc testing) are reported in Figure 5*d*.

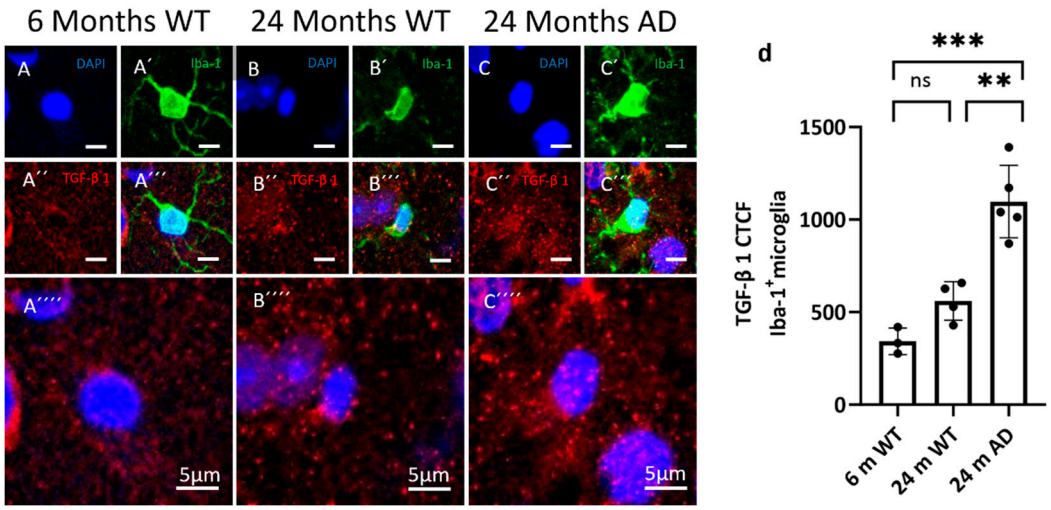

Figure 5. Distribution of TGF-β1 in microglia. Representative confocal images from cortex showing microglia and TGF-β1 in 6-month WT, 24-month WT, and 24-month APP/PS1 mice. Iba-1 marks microglia (green, A′, B′, C′), and TGF-β1 (red, A′′, B′′, C′′), nuclei are counterstained with DAPI (blue, A, B, C). (d) Quantification of corrected total cell fluorescence (CTCF) for TGF-β1 within Iba-1⁺ microglia. Data are shown as individual animals with mean ± SEM. Statistical significance was assessed by one-way ANOVA with Tukey's post hoc test: $p < 0.01$, $p < 0.001$; ns, not significant.

Downstream, we assessed R-SMAD phosphorylation as a readout of pathway engagement. In cortical microglia, pSMAD2 immunoreactivity was predominantly cytoplasmic with comparatively weaker nuclear accumulation in aged groups, indicative of impaired nuclear translocation (Figure 6*a–c*). Quantification of compartmental signals (DAPI-segmented nuclei and cytoplasm defined as Iba-1 mask minus nucleus) showed a shift of the nuclear/cytoplasmic (N/C) pSMAD2 ratio toward cytoplasmic predominance in both 24-month WT in 24-month APP/PS1 mice relative to 6-month WT controls (Figure 6*d–f*).

 doi:10.20944/preprints202512.0809.v1

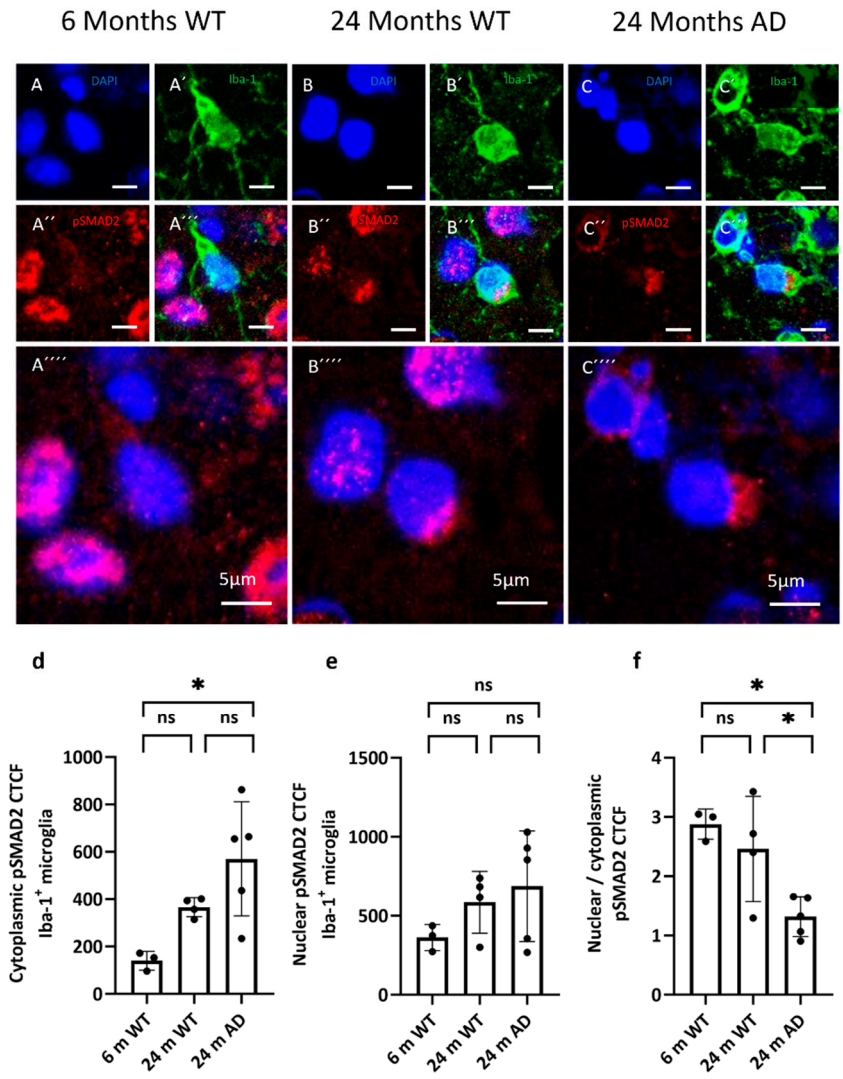

Figure 6. Distribution of pSMAD2 in microglia. (a–c) Representative confocal images from cortex showing phosphorylated SMAD2 (pSMAD2, red, A´´, B´´, C´´) in 6-month WT, 24-month WT, and 24-month APP/PS1 mice. Microglia are labeled with Iba-1 (green, A′, B′, C′) and nuclei with DAPI (blue, A, B, C). (d + e) Quantification of cytoplasmic and nuclear pSMAD2 CTCF within Iba-1⁺ microglia. (f) Nuclear/cytoplasmic (N/C) pSMAD2 ratio per cell (values >1 indicate nuclear enrichment; <1 indicate cytoplasmic predominance). Statistical significance was assessed by one-way ANOVA with Tukey's post hoc test: $p < 0.05$; ns, not significant.

To test whether this pattern generalized across the canonical branch, we analyzed pSMAD1/5/8 distributions (Figure 7). Quantification of pSMAD1/5/8 immunoreactivity in cortical microglia revealed a marked age-dependent increase in both cytoplasmic and nuclear signal intensity. Cytoplasmic pSMAD1/5/8 CTCF was significantly higher in 24-month WT and APP/PS1 mice compared with 6-month WT animals, with no additional increase in the AD group beyond age-matched controls (Figure 7*d*). A similar pattern was observed for nuclear pSMAD1/5/8, which was elevated in both aged groups relative to young WT (Figure 7*e*). In contrast, the nuclear-to-cytoplasmic pSMAD1/5/8 ratio remained unchanged across all three groups, indicating that aging and APP/PS1 pathology increase overall pSMAD1/5/8 levels but do not appreciably alter its subcellular partitioning (Figure 7*f*).

However, there is a significant difference between 6-month and 24-months WT microglia with a strong rise of cytoplasmic and nuclear Smad1/5/8 expression in the aged WT cells (Figure 7*d+e*).

Together, the compartmental data indicate a convergent shift toward cytoplasmic retention and/or diminished nuclear import of R-SMADs in aging and APP/PS1 cortex. Thus, while ligand and phospho-signals are detectable—and even elevated near plaques—the nuclear delivery step appears

 doi:10.20944/preprints202512.0809.v1

curtailed, consistent with a decoupling between receptor-proximal activation and transcriptional execution in plaque-associated, reactive microglia.

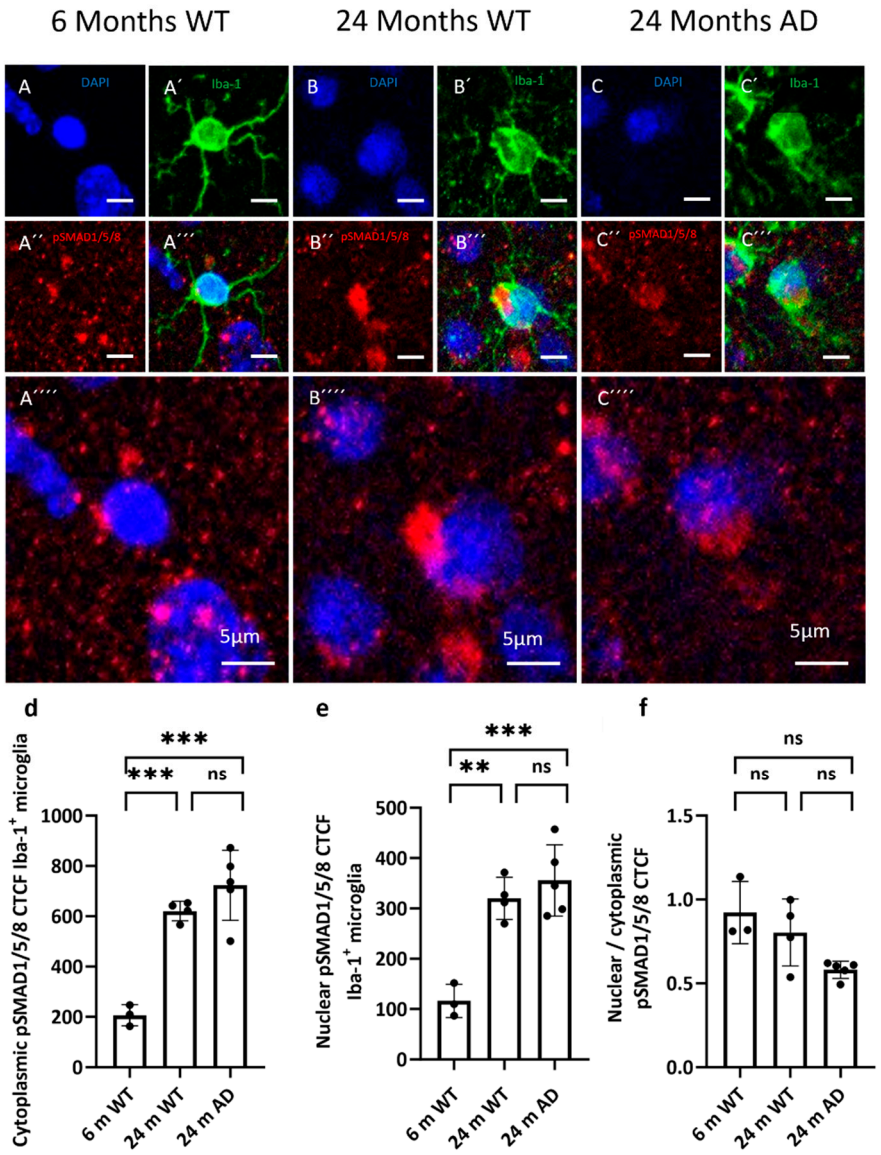

Figure 7. Distribution of pSMADs 1, 5 and 8 in microglia. (a–c) Representative confocal images from cortex showing phosphorylated SMADs1, 5 and 8 (red) in 6-month WT, 24-month WT, and 24-month APP/PS1 mice. Microglia are labeled with Iba-1 (green) and nuclei with DAPI (blue). (d + e) Quantification of cytoplasmic and nuclear pSMADs CTCF within Iba-1⁺ microglia. (f) Nuclear/cytoplasmic (N/C) pSMADs ratio per cell (values >1 indicate nuclear enrichment; <1 indicate cytoplasmic predominance). Statistical significance was assessed by one-way ANOVA with Tukey's post hoc test. The nuclear-to-cytoplasmic pSMAD1/5/8 CTCF ratio was analyzed using a Kruskal–Wallis test followed by Dunn's multiple comparisons test. Significance: $p < 0.01$, $p < 0.001$; ns, not significant.

3.4. Microglia Transcriptional Context

To place our morphological and signaling data into a broader molecular context, we re-analyzed the microglial RNA-sequencing dataset from Hemonnot-Girard et al., which reports pseudocount expression values for control microglia (CM), plaque-distant microglia (PCM), and plaque-associated microglia (PAM) at 4, 8, and 12 months of age [26]. Within this framework, CM represent microglia

 doi:10.20944/preprints202512.0809.v1

from non-amyloid controls, PCM reflect cells located away from plaques in Aβ mice, and PAM correspond to microglia directly associated with plaques.

As expected, classical homeostatic genes were most strongly expressed in CM and PCM, whereas plaque-associated PAM adopted a more disease-associated profile. *P2ry12* and *Tmem119* showed high average expression in CM and PCM and were reduced in PAM, particularly at 12 months of age. To characterize the DAM transcriptional profile, we examined the expression of key DAM markers (*Apoe, Trem2, Tyrobp, Cst7*) across CM, PCM and PAM at different stages of amyloid-β pathology (Figure 8). While *Apoe* was already low expressed in CM and PCM, it was further elevated in PAM at 8 and 12-months of age, consistent with a prominent activation of the APOE-driven DAM program in plaque-associated microglia. *Trem2* and *Tyrobp* followed a similar pattern, with relatively low expression in CM, intermediate levels in PCM, and the highest levels in PAM, reflecting progressive engagement of the TREM2–TYROBP axis in the plaque niche.

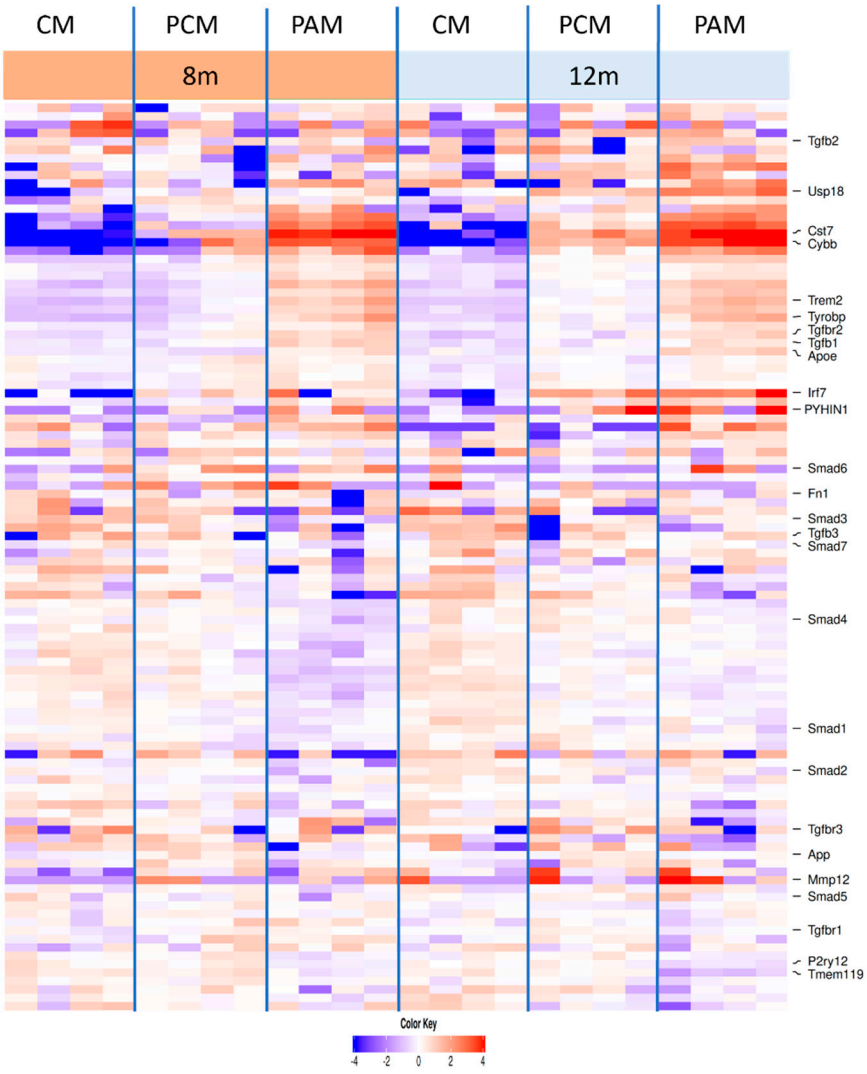

Figure 8. Microglial gene expression across all animals, groups, and ages. Heatmap showing the expression of selected homeostatic markers (*Tmem119, P2ry12*), TGF-β receptors and ligands (*Tgfbr1–3, Tgfb1–3*), SMAD signaling components (*Smad1, Smad2, Smad3, Smad4, Smad5, Smad6* and *Smad7*), and DAM markers (*Apoe, Tyrobp, Trem2, Cst7*) as well as TGF-β target genes (*Fn1, Smad7, Tgfb1, Tmem119*) in microglia classified as control microglia (CM), plaque-distant microglia (PCM) and plaque-associated microglia (PAM) at 8 and 12 months. Each column represents a single microglial sample (n = 4 per group and time point) from the dataset of Hemonnot-Girard *et al.* (Table S3). Values represent z-scores of log10(pseudocount + 1) expression per gene across all samples, with blue indicating relatively low and red relatively high expression.

 doi:10.20944/preprints202512.0809.v1

The cytochrome b-245 (*Cybb*) and the lysosomal cysteine protease inhibitor *Cst7* showed the most striking plaque-associated upregulation. Both genes were weakly expressed in CM and only moderately increased in PCM, but strongly induced in PAM, where they clearly segregated PAM from PCM. Together, this marker profile confirms that PAM adopt a robust DAM-like transcriptional state, characterized by activation of the TREM2–APOE–TYROBP module and pronounced upregulation of *Cybb* and *Cst7*, distinguishing them functionally and molecularly from both control and plaque-distant microglia. Regarding the neuroinflammatory profile, markers involved in interferon signaling, such as *Irf7*, *Usp18* and *Pyhin1*, are predominantly upregulated in 12-month PAM. In addition to interferon-related genes, plaque-associated microglia showed increased expression of *Mmp12*, a macrophage metalloelastase implicated in matrix degradation and chronic neuroinflammation, further supporting a shift toward a tissue-remodeling, pro-inflammatory microglial phenotype in the amyloid niche.

Apoc1 encodes apolipoprotein C-I, a component of lipoprotein particles that modulates lipid and cholesterol metabolism, and its upregulation in plaque-associated microglia is consistent with a lipid-remodeling, ApoE-linked DAM phenotype in the amyloid plaque niche.

We then focused on components of the TGF-β signaling pathway. Tgfb1 expression increased from CM to PCM and was further elevated in PAM, particularly at intermediate disease stages, indicating enhanced TGF-β ligand availability in plaque-associated microglia. Tgfb2 showed a similar, though more moderate, increase from CM through PCM to PAM, whereas Tgfb3 remained relatively stable or even slightly reduced in the PAM population. Among receptors, Tgfbr1 displayed a gradual rise from CM to PCM and PAM, while Tgfbr2 showed a more pronounced plaque-related gradient, with clearly higher expression in PCM and the highest levels in PAM at later stages. These patterns indicate that plaque-associated microglia not only up-regulate DAM markers, but also express increased levels of key TGF-β ligands and receptors, particularly Tgfb1 and Tgfbr2.

Core SMAD transcripts were largely maintained across conditions, but with notable shifts for specific members. Smad1, Smad2 and Smad5 showed broadly similar expression in CM, PCM and PAM, with only modest increases in plaque-associated cells. In contrast, Smad3 tended to be reduced in PAM compared to CM and PCM, consistent with a relative depletion of this canonical TGF-β R-SMAD in plaque-associated microglia. Smad4 was slightly higher in PCM than in CM and PAM, whereas the inhibitory regulator Smad7 remained at comparable levels across all three populations. Thus, the transcriptional landscape in plaque-associated microglia combines increased expression of TGF-β ligands and receptors with relatively lower Smad3 levels, suggesting a subtle imbalance between upstream receptor availability and downstream canonical SMAD transcription factors (Figure 8).

4. Discussion

This study demonstrates that aging and amyloid-β pathology jointly reshape microglial structure and signaling, with convergent effects on TGF-β/SMAD pathways and disease-associated gene expression. At the morphological level, we observe a progressive simplification of microglial arborization in aged and APP/PS1 mice, characterized by reduced branch points, endpoints and ramification index. Young microglia display a highly ramified, surveillant morphology, whereas microglia in 24-month WT and APP/PS1 animals adopt a more compact, hypertrophic shape with shorter and fewer processes. Notably, the extent of morphological simplification in APP/PS1 microglia does not markedly exceed that of age-matched WT animals, indicating that aging alone drives substantial structural remodeling of the microglial network. These findings align with the concept of “inflammaging”, in which age-related low-grade inflammation and chronic stress gradually erode the homeostatic microglial phenotype and lower the threshold for pathological activation [27].

Despite broadly similar morphology, prior transcriptomic work has shown that microglia in APP/PS1 models diverge functionally from aged WT counterparts, acquiring a distinct DAM profile characterized by upregulation of *Trem2*, *Apoe*, *Itgax* and *Cst7* and loss of homeostatic markers such as

 doi:10.20944/preprints202512.0809.v1

P2ry12 and *Tmem119* [17]. Our data are consistent with this view. The increased density of Iba-1⁺ microglia in 24-month APP/PS1 cortex (Figure 2), together with their plaque-associated, hypertrophic morphology, suggests that aging provides the structural substrate onto which amyloid pathology imprints a specialized, plaque-engaged state. The TREM2–TYROBP axis has been identified as a central driver of this transition, integrating lipid and damage-associated cues and promoting phagocytic, DAM-like programs [28,29]. It is therefore plausible that, even in the presence of similar arbor simplification, APP/PS1 microglia are functionally distinct from aged WT cells due to additional TREM2-dependent reprogramming in the amyloid niche.

At the level of TGF-β signaling, we find clear evidence for disease-related alterations. Microglial TGF-β1 protein levels are highest in 24-month APP/PS1 mice, indicating that plaque-engaged microglia are exposed to enhanced TGF-β ligand availability [29]. Our analysis of TGF-β pathway activity revealed more complex changes downstream. In cortical microglia, pSMAD2 immunoreactivity displays a predominantly cytoplasmic distribution in the aged AD-group, with comparatively weaker nuclear accumulation.

Quantitative analysis of nuclear versus cytoplasmic pSMAD2 CTCF supports a model of impaired nuclear translocation: despite robust cytoplasmic signal and local enrichment around plaques, nuclear pSMAD2 remains relatively low in aged APP/PS1 microglia. Together with the increased TGF-β1 and TGFBR2 expression observed in plaque-associated microglia, this pattern suggests a decoupling between strong upstream pathway activation and incomplete canonical nuclear SMAD2 output.

Our re-analysis of the Hemonnot-Girard bulk RNA-seq dataset provides independent support for this interpretation [26]. Focusing on microglial subclusters classified as CM, PCM and PAM at different disease stages, we find that PAM adopt a robust DAM-like transcriptional signature characterized by loss of homeostatic genes (*P2ry12, Tmem119*), strong induction of *Apoe, Trem2, Tyrobp* and *Cst7*, and increased expression of *Tgfb1* and *Tgfbr2* relative to CM and PCM. Thus, plaque-associated microglia appear to experience high TGF-β ligand and receptor availability in parallel with a full DAM program [29,30].

At the same time, canonical SMAD composition is subtly altered: while several SMAD family members (*Smad1, Smad2, Smad5*) remain relatively stable or show only modest increases, *Smad3* tends to be reduced in PAM compared with CM and PCM (Figure 8). Given the critical role of SMAD3 as an R-SMAD in the canonical TGF-β pathway, its relative depletion provides a plausible transcriptional correlate of the reduced nuclear pSMAD2 accumulation observed histologically.

Taken together, these data support a model in which plaque-associated microglia receive strong TGF-β input (increased *Tgfb1, Tgfbr2*, robust cytoplasmic pSMAD2 and peri-plaque enrichment), but transmit this signal only partially into canonical nuclear SMAD2/3-dependent transcription, in part due to altered SMAD3 availability [31]. In this scenario, TGF-β signaling may be sufficient to sustain aspects of the DAM phenotype and limit overt cytotoxicity, but insufficient to fully engage the homeostatic, anti-inflammatory and synapse-supporting programs typically associated with microglial TGF-β signaling in the healthy brain.

The selective vulnerability of the SMAD2/3 branch contrasts with our observations on pSMAD1/5/8. Both cytoplasmic and nuclear pSMAD1/5/8 levels are significantly elevated in microglia from 24-month WT and APP/PS1 mice compared with young WT animals, yet the nuclear-to-cytoplasmic ratio remains unchanged across groups. This indicates that aging and amyloid pathology globally increase SMAD1/5/8 signaling in microglia, while preserving the balance between cytoplasmic and nuclear localization. Given that SMAD1/5/8 are classically associated with BMP rather than TGF-β ligands, this pattern suggests that the BMP–SMAD axis remains functionally competent and may even be upregulated in the aged and amyloid-bearing cortex [32,33]. Enhanced SMAD1/5/8 activity could support tissue remodeling or survival responses, but it might also contribute to maladaptive matrix degradation and gliosis, depending on the downstream gene programs engaged [34,35]. Importantly, the preserved nuclear access of pSMAD1/5/8 argues against a global failure of SMAD trafficking and instead points to a selective impairment of the TGF-β–

 doi:10.20944/preprints202512.0809.v1

SMAD2/3 arm, consistent with studies showing that linker-region phosphorylation and MAPK-dependent modification of SMAD2/3 can specifically inhibit their nuclear translocation and canonical TGF-β signaling [36].

Several mechanisms could account for this dissociation between upstream TGF-β activation and downstream SMAD2/3 function. One possibility is direct sequestration or mislocalization of SMAD proteins by pathological aggregates such as hyperphosphorylated Tau, as suggested in other tauopathy models. Another, not mutually exclusive explanation is cross-regulation by competing signaling cascades. The ERK/MAPK pathway can inhibit SMAD nuclear translocation by phosphorylating linker regions within SMAD proteins [37], and ERK/MAPK activity is known to be increased in AD [38]. Moreover, pharmacological inhibition of EGFR/MAPK signaling reduces pro-inflammatory microglial activation in experimental systems [39].

In plaque-associated microglia, where we observe strong DAM activation, upregulation of interferon-related genes (*Irf7*, *Usp18*, *Pyhin1*), increased expression of proteolytic and matrix-remodeling factors such as *Mmp12*, and lipid-associated genes including *Apoc1*, it is conceivable that MAPK and interferon pathways compete with or override canonical TGF-β–SMAD2/3 signaling [40,41]. Reduced SMAD activity would then not solely reflect intrinsic defects in the TGF-β pathway, but also the influence of these converging pro-inflammatory networks.

Our findings therefore place TGF-β/SMAD signaling into a broader context of microglial state transitions in aging and AD. Aging alone induces morphological simplification and increases overall SMAD1/5/8 activity, while preserving a more homeostatic transcriptomic profile. The addition of amyloid pathology drives microglia into a PAM/DAM state with pronounced TREM2–TYROBP activation, interferon signaling, lipid remodeling and upregulated TGF-β ligand and receptor expression. Within this state, the canonical TGF-β–SMAD2/3 axis appears to be partially uncoupled, with high upstream input but incomplete nuclear output. This imbalance may stabilize a chronically reactive, plaque-engaged phenotype that is only partially restrained by endogenous anti-inflammatory and pro-homeostatic signals.

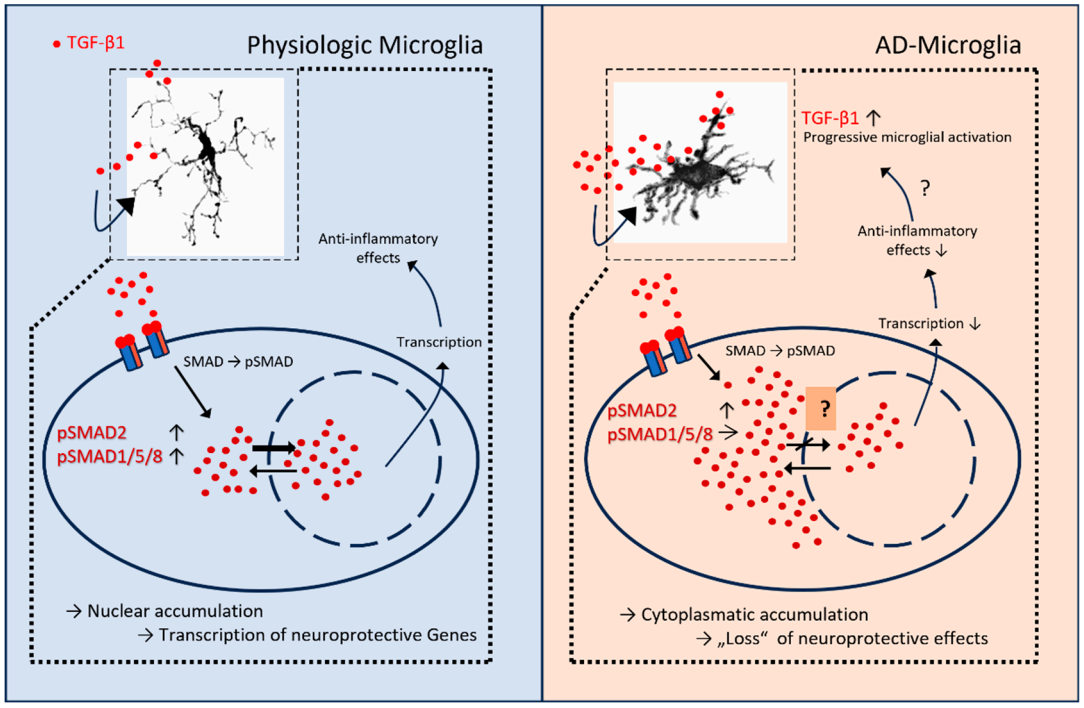

Figure 9. Proposed model of TGF-β/SMAD signaling in physiologic versus AD microglia. Left, physiologic microglia: TGF-β1 engages its receptors, leading to SMAD phosphorylation and balanced nuclear accumulation of pSMAD2 and pSMAD1/5/8. Nuclear SMAD complexes cooperate with transcription factors to drive neuroprotective, anti-inflammatory gene programs. Right, AD microglia: despite increased extracellular TGF-

 doi:10.20944/preprints202512.0809.v1

β1 and receptor engagement, pSMAD2 shows predominant cytoplasmic retention with comparatively weaker nuclear accumulation, resulting in reduced transcriptional output and diminished anti-inflammatory effects; pSMAD1/5/8 remains detectable. Insets depict representative microglial morphologies in the respective conditions. Arrows summarize the shift from nuclear to cytoplasmic pSMAD2 and the putative loss of TGF-β-mediated neuroprotection in AD microglia. Graphic was designed with Microsoft Power Point.

Several limitations of our study should be acknowledged. First, our morphological and signaling analyses are based on a relatively small number of animals and a cross-sectional design, which precludes firm conclusions about temporal causality between amyloid deposition, TGF-β signaling changes, and microglial remodeling. Second, our quantification of pSMAD localization relies on immunofluorescence and corrected total cell fluorescence; while informative, this approach cannot fully capture dynamic signaling kinetics or resolve microglial subpopulations beyond Iba-1 positivity. Third, our transcriptomic conclusions are derived from re-analysis of a published single-cell dataset; although this dataset is well annotated and highly informative, it represents one specific APP/PS1 model and may not encompass the full spectrum of microglial states across brain regions and disease stages. Finally, we did not directly manipulate TGF-β/SMAD or MAPK pathways *in vivo*, so the causal contribution of these signaling changes to microglial function and neurodegeneration remains to be established.

Despite these limitations, our combined structural, signaling and transcriptomic analyses highlight morphological degeneration and altered TGF-β/SMAD signaling in microglia as key features of the aged and Alzheimer's brain. Plaque-associated microglia emerge as structurally simplified yet transcriptionally hyperactive cells that integrate strong TREM2–TYROBP, interferon and TGF-β inputs, but relay only an incomplete canonical SMAD2/3 response. Modulating this imbalanced signaling landscape—either by restoring effective nuclear SMAD2/3 translocation or by dampening competing pro-inflammatory cascades such as ERK/MAPK and interferon pathways—may help re-establish glial neuroprotective functions and potentially slow disease progression.

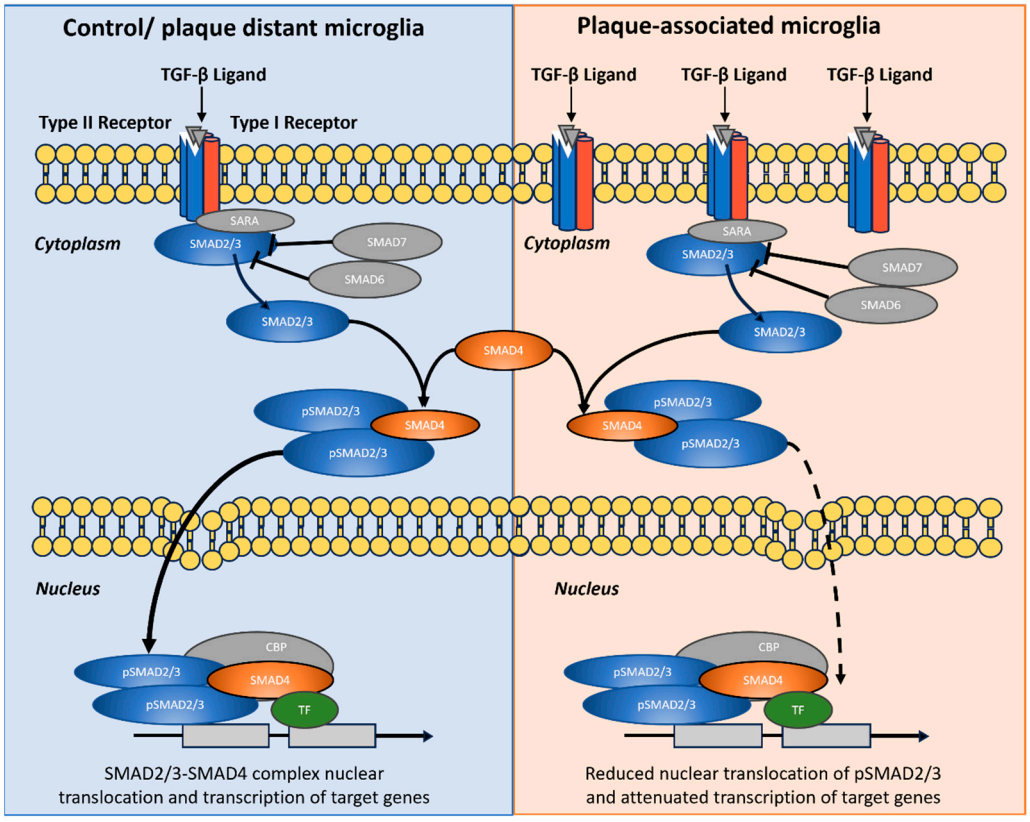

Figure 10. Graphical summary of hypothesized role of TGF-β/SMAD2/3 signaling in control/plaque-distant microglia versus attenuated nuclear output in plaque-associated microglia. Schematic comparison of pathway

 doi:10.20944/preprints202512.0809.v1

organization and subcellular routing. Left (Control/plaque-distant microglia): TGF-β ligand binding to type II/I receptors recruits SMAD2/3 via SARA, leading to receptor-mediated phosphorylation (pSMAD2/3), assembly with SMAD4, nuclear translocation, and transcriptional activation with TF/CBP co-factors. Inhibitory SMADs (SMAD6/7) are shown as pathway brakes. Right (Plaque-associated microglia): Despite multiple receptor–ligand engagements at the membrane and robust cytoplasmic pSMAD2/3 formation, nuclear import of SMAD2/3–SMAD4 complexes is reduced (dashed arrow), resulting in attenuated transcriptional output. The diagram illustrates the decoupling between strong upstream activation and diminished canonical nuclear SMAD2/3 signaling in plaque-associated microglia. Graphic was designed with Microsoft Power Point.

Future work combining high-resolution morphometrics with spatial transcriptomics and targeted pathway manipulation will be essential to dissect how these intertwined signaling networks shape microglial behavior in the aging and amyloid-affected brain and to identify points of therapeutic leverage within the TGF-β/SMAD pathway.

Supplementary Materials: The following supporting information can be downloaded at the website of this paper posted on Preprints.org.

Author Contributions: Conceptualization, B.S. and N.V.; methodology, O.K.; software, O.K.; resources, A.K. and B.S.; writing—original draft preparation, N.V. and O.K.; writing—review and editing, N.V., O.K., A.K. and B.S.; visualization, N.V. and O.K..; supervision, B.S.; project administration, N.V.; funding acquisition, B.S. All authors have read and agreed to the published version of the manuscript. Please turn to the CRediT taxonomy for the term explanation. Authorship must be limited to those who have contributed substantially to the work reported.

Funding: DFG: grant number: SP 1555/2-3 for B.S.

Institutional Review Board Statement: The present study was carried out in accordance with the European Communities Council Directive of September 22nd 2010 (2010/63/EEC) for care of laboratory animals. The breeding was approved by the local Animal Research Committee (Landesamt für Landwirtschaft, Lebensmittelsicherheit und Fischerei (LALLF)) of the state Mecklenburg-Western Pomerania (LALLF M-V/TSD/7221.3-2-034/17).

Informed Consent Statement: Not applicable.

Data Availability Statement: For the study transcriptomic analysis, publicly available data was re-analyzed from Hemonnot-Girard *et al.*, Table S3, accession GSE205048.

Acknowledgments: The authors cordially thank the technicians of the Central Animal Care Facility, Rostock University Medical Center.

Conflicts of Interest: The authors declare no conflicts of interest.

Abbreviations

The following abbreviations are used in this manuscript:

MDPI	Multidisciplinary Digital Publishing Institute
DOAJ	Directory of open access journals
TLA	Three letter acronym
LD	Linear dichroism

References

1. Lo, M.W.; Woodruff, T.M. Complement: Bridging the Innate and Adaptive Immune Systems in Sterile Inflammation. *J. Leukoc. Biol.* **2020**, *108*, 339–351, doi:10.1002/JLB.3MIR0220-270R.

 doi:10.20944/preprints202512.0809.v1

2. Arnold, T.D.; Lizama, C.O.; Cautivo, K.M.; Santander, N.; Lin, L.; Qiu, H.; Huang, E.J.; Liu, C.; Mukouyama, Y.; Reichardt, L.F.; et al. Impaired αVβ8 and TGFβ Signaling Lead to Microglial Dysmaturation and Neuromotor Dysfunction. *J. Exp. Med.* **2019**, *216*, 900–915, doi:10.1084/jem.20181290.
3. Zöller, T.; Schneider, A.; Kleimeyer, C.; Masuda, T.; Potru, P.S.; Pfeifer, D.; Blank, T.; Prinz, M.; Spittau, B. Silencing of TGFβ Signalling in Microglia Results in Impaired Homeostasis. *Nat. Commun.* **2018**, *9*, 4011, doi:10.1038/s41467-018-06224-y.
4. Hao, M.; Chen, J. Trend Analysis and Future Predictions of Global Burden of Alzheimer's Disease and Other Dementias: A Study Based on the Global Burden of Disease Database from 1990 to 2021. *BMC Med.* **2025**, *23*, 378, doi:10.1186/s12916-025-04169-w.
5. 2025 Alzheimer's Disease Facts and Figures. *Alzheimers Dement.* **2025**, *21*, e70235, doi:10.1002/alz.70235.
6. Coppens, S.; Lehmann, S.; Hopley, C.; Hirtz, C. Neurofilament-Light, a Promising Biomarker: Analytical, Metrological and Clinical Challenges. *Int. J. Mol. Sci.* **2023**, *24*, 11624, doi:10.3390/ijms241411624.
7. Kenaan, N.; Alshehabi, Z. A Review on Recent Advances in Alzheimer's Disease: The Role of Synaptic Plasticity. *AIMS Neurosci.* **2025**, *12*, 75–94, doi:10.3934/Neuroscience.2025006.
8. Kayed, R.; Lasagna-Reeves, C.A. Molecular Mechanisms of Amyloid Oligomers Toxicity. *J. Alzheimers Dis. JAD* **2013**, *33 Suppl 1*, S67-78, doi:10.3233/JAD-2012-129001.
9. Heppner, F.L.; Ransohoff, R.M.; Becher, B. Immune Attack: The Role of Inflammation in Alzheimer Disease. *Nat. Rev. Neurosci.* **2015**, *16*, 358–372, doi:10.1038/nrn3880.
10. Sobue, A.; Komine, O.; Hara, Y.; Endo, F.; Mizoguchi, H.; Watanabe, S.; Murayama, S.; Saito, T.; Saido, T.C.; Sahara, N.; et al. Microglial Gene Signature Reveals Loss of Homeostatic Microglia Associated with Neurodegeneration of Alzheimer's Disease. *Acta Neuropathol. Commun.* **2021**, *9*, 1, doi:10.1186/s40478-020-01099-x.
11. Lee, C.Y.D.; Landreth, G.E. The Role of Microglia in Amyloid Clearance from the AD Brain. *J. Neural Transm. Vienna Austria 1996* **2010**, *117*, 949–960, doi:10.1007/s00702-010-0433-4.
12. Spittau, B.; Dokalis, N.; Prinz, M. The Role of TGFβ Signaling in Microglia Maturation and Activation. *Trends Immunol.* **2020**, *41*, 836–848, doi:10.1016/j.it.2020.07.003.
13. Vidovic, N.; Spittau, B. Microglial Transforming Growth Factor-β Signaling in Alzheimer's Disease. *Int. J. Mol. Sci.* **2024**, *25*, 3090, doi:10.3390/ijms25063090.
14. Inman, G.J.; Nicolás, F.J.; Hill, C.S. Nucleocytoplasmic Shuttling of Smads 2, 3, and 4 Permits Sensing of TGF-Beta Receptor Activity. *Mol. Cell* **2002**, *10*, 283–294, doi:10.1016/s1097-2765(02)00585-3.
15. Von Bernhardi, R.; Cornejo, F.; Parada, G.; Eugenin, J. Role of TGFβ Signaling in the Pathogenesis of Alzheimer's Disease. *Front. Cell. Neurosci.* **2015**, *9*, doi:10.3389/fncel.2015.00426.
16. Pettas, S.; Karagianni, K.; Kanata, E.; Chatziefstathiou, A.; Christoudia, N.; Xanthopoulos, K.; Sklaviadis, T.; Dafou, D. Profiling Microglia through Single-Cell RNA Sequencing over the Course of Development, Aging, and Disease. *Cells* **2022**, *11*, 2383, doi:10.3390/cells11152383.
17. Keren-Shaul, H.; Spinrad, A.; Weiner, A.; Matcovitch-Natan, O.; Dvir-Szternfeld, R.; Ulland, T.K.; David, E.; Baruch, K.; Lara-Astaiso, D.; Toth, B.; et al. A Unique Microglia Type Associated with Restricting Development of Alzheimer's Disease. *Cell* **2017**, *169*, 1276-1290.e17, doi:10.1016/j.cell.2017.05.018.
18. Liu, W.; Taso, O.; Wang, R.; Bayram, S.; Graham, A.C.; Garcia-Reitboeck, P.; Mallach, A.; Andrews, W.D.; Piers, T.M.; Botia, J.A.; et al. Trem2 Promotes Anti-Inflammatory Responses in Microglia and Is Suppressed under pro-Inflammatory Conditions. *Hum. Mol. Genet.* **2020**, *29*, 3224–3248, doi:10.1093/hmg/ddaa209.
19. Lok, K.; Zhao, H.; Shen, H.; Wang, Z.; Gao, X.; Zhao, W.; Yin, M. Characterization of the APP/PS1 Mouse Model of Alzheimer's Disease in Senescence Accelerated Background. *Neurosci. Lett.* **2013**, *557*, 84–89, doi:10.1016/j.neulet.2013.10.051.
20. Reinders, N.R.; Spek, S.J.F. van der; Klaassen, R.V.; Koymans, K.J.; MacGillavry, H.D.; Smit, A.B.; Kessels, H.W. Amyloid-β-Driven Synaptic Deficits Are Mediated by Synaptic Removal of GluA3-Containing AMPA Receptors. *J. Neurosci.* **2025**, *45*, doi:10.1523/JNEUROSCI.0393-24.2024.
21. Oshima, T.; Kater, M.S.J.; Huffels, C.F.M.; Wesseling, E.M.; Middeldorp, J.; Hol, E.M.; Verheijen, M.H.G.; Smit, A.B.; Boddeke, E.W.G.M.; Eggen, B.J.L. Early Amyloid-Induced Changes in Microglia Gene Expression in Male APP/PS1 Mice. *J. Neurosci. Res.* **2024**, *102*, e25295, doi:10.1002/jnr.25295.

 doi:10.20944/preprints202512.0809.v1

22. Jankowsky, J.L.; Fadale, D.J.; Anderson, J.; Xu, G.M.; Gonzales, V.; Jenkins, N.A.; Copeland, N.G.; Lee, M.K.; Younkin, L.H.; Wagner, S.L.; et al. Mutant Presenilins Specifically Elevate the Levels of the 42 Residue Beta-Amyloid Peptide in Vivo: Evidence for Augmentation of a 42-Specific Gamma Secretase. *Hum. Mol. Genet.* **2004**, *13*, 159–170, doi:10.1093/hmg/ddh019.
23. Schnell, S.A.; Staines, W.A.; Wessendorf, M.W. Reduction of Lipofuscin-like Autofluorescence in Fluorescently Labeled Tissue. *J. Histochem. Cytochem. Off. J. Histochem. Soc.* **1999**, *47*, 719–730, doi:10.1177/002215549904700601.
24. Arshadi, C.; Günther, U.; Eddison, M.; Harrington, K.I.S.; Ferreira, T.A. SNT: A Unifying Toolbox for Quantification of Neuronal Anatomy. *Nat. Methods* **2021**, *18*, 374–377, doi:10.1038/s41592-021-01105-7.
25. El-Sharkawey, A. Calculate the Corrected Total Cell Fluorescence (CTCF). 2016.
26. Hemonnot-Girard, A.-L.; Meersseman, C.; Pastore, M.; Garcia, V.; Linck, N.; Rey, C.; Chebbi, A.; Jeanneteau, F.; Ginsberg, S.D.; Lachuer, J.; et al. Comparative Analysis of Transcriptome Remodeling in Plaque-Associated and Plaque-Distant Microglia during Amyloid-β Pathology Progression in Mice. *J. Neuroinflammation* **2022**, *19*, 234, doi:10.1186/s12974-022-02581-0.
27. Franceschi, C.; Garagnani, P.; Parini, P.; Giuliani, C.; Santoro, A. Inflammaging: A New Immune-Metabolic Viewpoint for Age-Related Diseases. *Nat. Rev. Endocrinol.* **2018**, *14*, 576–590, doi:10.1038/s41574-018-0059-4.
28. Krasemann, S.; Madore, C.; Cialic, R.; Baufeld, C.; Calcagno, N.; El Fatimy, R.; Beckers, L.; O'Loughlin, E.; Xu, Y.; Fanek, Z.; et al. The TREM2-APOE Pathway Drives the Transcriptional Phenotype of Dysfunctional Microglia in Neurodegenerative Diseases. *Immunity* **2017**, *47*, 566-581.e9, doi:10.1016/j.immuni.2017.08.008.
29. Audrain, M.; Haure-Mirande, J.-V.; Mleczko, J.; Wang, M.; Griffin, J.K.; St George-Hyslop, P.H.; Fraser, P.; Zhang, B.; Gandy, S.; Ehrlich, M.E. Reactive or Transgenic Increase in Microglial TYROBP Reveals a TREM2-Independent TYROBP-APOE Link in Wild-Type and Alzheimer's-Related Mice. *Alzheimers Dement. J. Alzheimers Assoc.* **2021**, *17*, 149–163, doi:10.1002/alz.12256.
30. Haure-Mirande, J.-V.; Audrain, M.; Ehrlich, M.E.; Gandy, S. Microglial TYROBP/DAP12 in Alzheimer's Disease: Transduction of Physiological and Pathological Signals across TREM2. *Mol. Neurodegener.* **2022**, *17*, 55, doi:10.1186/s13024-022-00552-w.
31. Yang, C.; Xu, P. The Role of Transforming Growth Factor B1 /Smad Pathway in Alzheimer's Disease Inflammation Pathology. *Mol. Biol. Rep.* **2023**, *50*, 777–788, doi:10.1007/s11033-022-07951-8.
32. Wu, M.; Wu, S.; Chen, W.; Li, Y.-P. The Roles and Regulatory Mechanisms of TGF-β and BMP Signaling in Bone and Cartilage Development, Homeostasis and Disease. *Cell Res.* **2024**, *34*, 101–123, doi:10.1038/s41422-023-00918-9.
33. Le Dréau, G. BuMPing Into Neurogenesis: How the Canonical BMP Pathway Regulates Neural Stem Cell Divisions Throughout Space and Time. *Front. Neurosci.* **2022**, *15*, 819990, doi:10.3389/fnins.2021.819990.
34. Yousef, H.; Morgenthaler, A.; Schlesinger, C.; Bugaj, L.; Conboy, I.M.; Schaffer, D.V. Age-Associated Increase in BMP Signaling Inhibits Hippocampal Neurogenesis. *Stem Cells Dayt. Ohio* **2015**, *33*, 1577–1588, doi:10.1002/stem.1943.
35. Ueki, Y.; Reh, T.A. Activation of BMP-Smad1/5/8 Signaling Promotes Survival of Retinal Ganglion Cells after Damage in Vivo. *PloS One* **2012**, *7*, e38690, doi:10.1371/journal.pone.0038690.
36. Kamato, D.; Do, B.H.; Osman, N.; Ross, B.P.; Mohamed, R.; Xu, S.; Little, P.J. Smad Linker Region Phosphorylation Is a Signalling Pathway in Its Own Right and Not Only a Modulator of Canonical TGF-β Signalling. *Cell. Mol. Life Sci. CMLS* **2020**, *77*, 243–251, doi:10.1007/s00018-019-03266-3.
37. Kretzschmar, M.; Doody, J.; Massagué, J. Opposing BMP and EGF Signalling Pathways Converge on the TGF-Beta Family Mediator Smad1. *Nature* **1997**, *389*, 618–622, doi:10.1038/39348.
38. Chen, M.J.; Ramesha, S.; Weinstock, L.D.; Gao, T.; Ping, L.; Xiao, H.; Dammer, E.B.; Duong, D.D.; Levey, A.I.; Lah, J.J.; et al. Extracellular Signal-Regulated Kinase Regulates Microglial Immune Responses in Alzheimer's Disease. *J. Neurosci. Res.* **2021**, *99*, 1704–1721, doi:10.1002/jnr.24829.
39. Qu, W.-S.; Tian, D.-S.; Guo, Z.-B.; Fang, J.; Zhang, Q.; Yu, Z.-Y.; Xie, M.-J.; Zhang, H.-Q.; Lü, J.-G.; Wang, W. Inhibition of EGFR/MAPK Signaling Reduces Microglial Inflammatory Response and the Associated Secondary Damage in Rats after Spinal Cord Injury. *J. Neuroinflammation* **2012**, *9*, 178, doi:10.1186/1742-2094-9-178.

 doi:10.20944/preprints202512.0809.v1

40. Goldmann, T.; Zeller, N.; Raasch, J.; Kierdorf, K.; Frenzel, K.; Ketscher, L.; Basters, A.; Staszewski, O.; Brendecke, S.M.; Spiess, A.; et al. USP18 Lack in Microglia Causes Destructive Interferonopathy of the Mouse Brain. *EMBO J.* **2015**, *34*, 1612–1629, doi:10.15252/embj.201490791.
41. Hansmann, F.; Zhang, N.; Herder, V.; Leitzen, E.; Baumgärtner, W. Delayed Astrogliosis Associated with Reduced M1 Microglia Activation in Matrix Metalloproteinase 12 Knockout Mice during Theiler's Murine Encephalomyelitis. *Int. J. Mol. Sci.* **2019**, *20*, 1702, doi:10.3390/ijms20071702.